Available online at www.sciencedirect.com
ScienceDirect
Trans. Nonferrous Met. Soc. China 32(2022) 3753−3766
Transactions of Nonferrous Metals Society of China
www.tnmsc.cn

Coordination configurations of cupric tartrate in electronic industry wastewater

Ming-jun HAN[1], Jian-yong HE[1], Wei SUN[1], Sai LI[1], Heng YU[1], Tong YUE[1], Xin WEI[2], Chen-yang ZHANG[1,3,4]

1. Key Laboratory of Hunan Province for Clean and Efficient Utilization of Strategic Calcium-containing Mineral Resources, School of Minerals Processing and Bioengineering, Central South University, Changsha 410083, China;
2. Suzhou Dongfang Environmental Engineering Co., Ltd., Suzhou 215110, China;
3. Key Laboratory of Hunan Province for Comprehensive Utilization of Complex Copper−Lead Zinc Associated Metal Resources, Hunan Research Institute for Nonferrous Metals, Changsha 410100, China;
4. State Key Laboratory of Complex Nonferrous Metal Resources Clean Utilization, Kunming University of Science and Technology, Kunming 650093, China

Received 1 October 2021; accepted 19 January 2022

Abstract: The coordination structure of cupric tartrate (Cu−TA) complex was investigated by ultraviolet−visible (UV−Vis) and liquid chromatography/mass spectrometer (LC−MS) firstly; furthermore, effective coordination configurations and electronic properties of Cu−TA in aqueous solution were systematically revealed by density functional theory (DFT) calculations. Consistently, Job plots show the possible existence of [Cu(TA)] and $[Cu(TA)_2]^{2-}$ at 230 and 255 nm based on UV−Vis results. LC−MS results confirm the existence of the single and high coordination complexes $[Cu_2(TA)_2]^+$, $[Cu(TA)_2]^+$ and $[Cu_2(TA)_3(H_2O)_2(OH)_2]^{2+}$. DFT calculation results show that carboxylic oxygen and hydroxyl oxygen of tartaric acid (TA) are preferred sites for Cu(II) coordination. [Cu(TA)] (1^H, 3^H sites O of TA coordinated with Cu(II)), $[Cu(TA)_2]^{2-}$ (two 1^C, 2^H sites O of TA coordinated with Cu(II)), and $[Cu(TA)_3]^{4-}$ (three 2^H, 3^H sites O of TA coordinated with Cu(II)) should be dominant coordination configurations of Cu−TA. The corresponding Gibbs reaction energies are −170.1, −136.2, and −90.2 kJ/mol, respectively.

Key words: electronic industry wastewater; copper; tartaric acid; cupric tartrate complex; coordination configuration; density functional theory

1 Introduction

Copper is an important non-ferrous metal widely used in the electronics industry [1,2]. Simultaneously, copper presents particularly high thermodynamic affinity and rapid metal−ligand bonding kinetics efficiency for typical nitrogen and oxygen chelating ligands [3,4]. Meanwhile, tartaric acid (TA) is a potential ligand with wide applications, such as complexing reagent in electroplating industry, additive in food industry, fixing reagent for textile printing and dyeing, and medical reagents in biomedical industry [5−8]. Oxygen atoms with lone electron pairs in TA molecules can be aligned with metal ions by chelating or bridging to form mononuclear, binuclear and polymeric complexes [9,10]. Stable chelate complex formed by TA with Cu(II) is called cupric tartrate ($[Cu(TA)_m]^{2m-2}$) [11], also known as copper dihydroxy succinate, which is widely used in electroplating and electroless plating practices. The production process inevitably produces a large amount of wastewater, including complexing

Corresponding author: Chen-yang ZHANG, Tel: +86-15573156566, E-mail: zhangchenyang@csu.edu.cn
DOI: 10.1016/S1003-6326(22)66055-2

reagents, such as TA, ethylene diamine tetraacetic acid (EDTA), and citric acid (CA) [12,13], a variety of heavy metals including copper, nickel, zinc, and iron [14,15], and the corresponding metal−organic complexes [16]. The coexisting contaminants of heavy metals and organic pollutants demonstrate complex morphology and high stability. As a result, ideal treatment effect is difficult to obtain using traditional water treatment methods and serious ecological environmental pollution can occur because wastewater shows characteristics of high acidity, high COD and multi-metal complex [17,18]. Advanced oxidation processes (AOPs) are typically used for treating heavy metal complexing wastewater to efficiently break strong chelation between metal ions and chelating reagent [19]. Ligands are oxidized and degraded into small molecules such as CO_2 and H_2O, resulting in metal ions release. Then, chemical precipitation, ion exchange, adsorption and other technologies are utilized to recover or purify metal ions in wastewater [20].

In addition, TA is also used to modify rice husk for adsorption of copper ions in aqueous solutions [21]. Cupric tartrate can also be directly used as an effective ingredient of Fehling's reagent to identify the presence of reducing sugars [22]. However, the serious lack of understanding of valence bond structure, active center and action essence of Cu−TA at the electronic level has greatly hindered its applicability. For instance, complexation characteristics of heavy metals and organic compounds in electroplating and electroless plating baths as well as decomplexation mechanism of advanced oxidation processes remain unclear. First-principles density functional theory (DFT) is a classical theoretical method in quantum chemistry, which has become an effective tool for microscopic studies in physics, chemistry, materials, and biomedicine disciplines [23,24]. Solving production problems in practice and understanding existence state and action essence between substances through electronic structure are important [25,26]. Therefore, first-principles DFT calculations demonstrate high application potential in clearly understanding difficult problems in fields of electronic information and environmental science.

Identifying the presence state of copper in wastewater is important in recycling metallic copper and the deep purification of wastewater. Accordingly, coordination configurations of Cu−TA complex, a representative refractory pollutant in electronic industry wastewater, were systematically explored by using UV−Vis spectrophotometry, LC−MS characterization techniques, and first-principles DFT calculations at the atomic scale in this study. The coordination mechanism of TA with Cu(II) was revealed from spectral technique and quantum chemistry calculations, including geometry structure, thermodynamic analysis, valence bond, Mayer bond order, electron localization function (ELF), electrostatic potential (ESP), and frontier molecular orbitals (MOs). This work would provide a systematical and deep understanding of coordination characteristics for electroplating and electroless plating active agents. It should also shed new insights into the resourceful treatment and deep purification of the electronic industry wastewater containing heavy metals−organic complexes.

2 Experiment and computation

2.1 Experiment

2.1.1 Materials

Tartaric acid and blue copperas (purity >99%) were purchased from Shanghai Macklin Biochemical Co., Ltd., China. Pure water (18.2 MΩ) produced by Arium Mini Plus (Sartorius Weighing Technology, Goettingen, Germany) was used in this work. The solution of Cu–TA was prepared by mixing tartaric acid with blue copperas, and the specific ratio was further explained in subsequent experiments.

2.1.2 UV−Vis tests

Ultraviolet spectrophotometry is a commonly-used characterization technique for monitoring the presence of complex compounds [14,27]. Method of continuous variations (MCV), also known as Method of Job [28], can provide qualitative and quantitative insights into stoichiometries of underlying associations of m molecules of A and n molecules of B to form A_mB_n. Therefore, MCV was used in this work to explore the proportions and possible forms of TA and Cu(II), and Job plots were applied to tracking the full reaction path and reflecting the essence of coordination reaction [29]. A Shimadzu UV−2600 ultraviolet−visible spectrophotometer was utilized to obtain the UV−Vis spectra at a fixed concentration using equimolar

continuous change method and molar ratio methods. Scanning speed was set to medium, wavelength range was 185−400 nm, and sampling interval was 0.1 nm.

2.1.3 LC−MS tests

The linear ion trap quadrupole liquid chromatography/mass spectrometer (LC−MS), model SCIEX Qtrap 6500+, was used to demonstrate the presence of compounds in the cupric tartrate solution. The sample effluent flowing through a probe was applied at a high voltage, where the Turbo V^{TM} ion source could ionize molecules in the solution to become charged gas phase ions, which were further analyzed using mass spectrometry. Molecular mass and structure information could be accurately quantified and provided through the charge state distribution. Positive polarity detection was performed at a mass-to-charge ratio range of 50−600 and scanning rate of 1000 Da/s for 5 min. Natural pH value and different stoichiometric ratios were selected to obtain a simple aqueous solution of Cu−TA structure, which was supposed to provide coordination evidence of Cu−TA complex.

2.2 Computation

2.2.1 Cluster models

The existence of two asymmetric carbon atoms in the molecular structure of tartaric acid, allows it to mainly exist in the form of L-tartaric acid, D-tartaric acid, Meso-tartaric acid, and DL-tartaric acid [30,31]. Among them, DL-tartaric acid is formed through the co-existence of L-tartaric acid and D-tartaric acid that cancel the optical activity of each other. The structures of L-tartaric acid, D-tartaric acid, and Meso-tartaric acid are shown in Fig. S1. L-tartaric acid is widely used in the production practice and adopted as the following research object.

Cu(II) was set as the metal center ion, which was the coordination center of bidentate TA anions. The proposed coordination conformations were composed of one, two, and three TA anions with a metal center ion, respectively. Furthermore, coordination configurations of single molecule and multiple molecules of TA^{2-} with a single Cu(II), binding sites of Cu(II) with TA^{2-} for each coordination, and the influence of explicit solvent H_2O were considered. As illustrated in Fig. 1, the following coordination configurations were preliminarily defined according to the valence bond properties of Cu(II) and the geometric arrangement of oxygen and carbon atoms in TA^{2-}: 1^C, 1^H sites O of TA coordinated with Cu(II); 1^C, 2^H sites O of TA coordinated with Cu(II); 2^H, 3^H sites O of TA coordinated with Cu(II); 1^H, 3^H sites O of TA coordinated with Cu(II); 1^C, 3^H sites O of TA coordinated with Cu(II), where H denotes hydroxyl oxygen and C denotes carboxyl oxygen.

2.2.2 Computational methods

The cluster models of $[Cu(TA)_m]^{2-2m}$ and $[Cu(TA)_m(H_2O)_n]^{2-2m}$ were built and optimized by GaussView 6.0 and Gaussian 16 A.03 [32], respectively. All calculations were performed via the DFT method using the functional of ωB97XD [33], with the all-electron basis set def2-SVP for light atoms H, C, and O, and def2-TZVP basis set for heavy atom Cu. Cupric tartrate chelate is a molecule with many branching structures, the distance between the coordination oxygen atom and the Cu(II) is relatively close, and dispersion cannot be ignored. Dispersion effects have been included in the ωB97XD functional, which uses a version of Grimme's D2 dispersion model [34]. Implicit solvation effects were considered using the solvation model based on

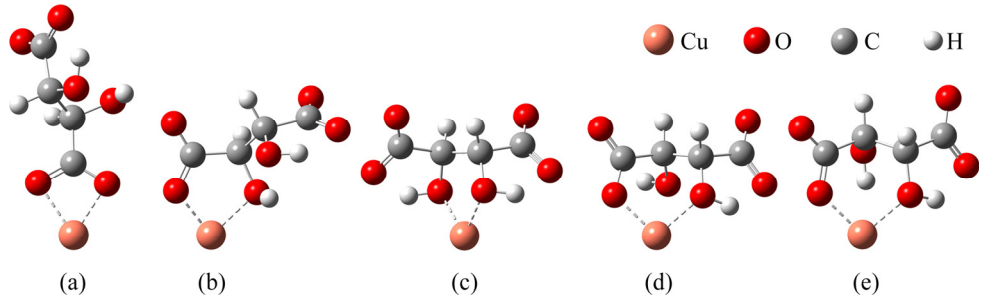

Fig. 1 Possible coordination sites of [Cu(TA)]: (a) 1^C, 1^H sites O of TA coordinated with Cu(II); (b) 1^C, 2^H sites O of TA coordinated with Cu(II); (c) 2^H, 3^H sites O of TA coordinated with Cu(II); (d) 1^H, 3^H sites O of TA coordinated with Cu(II); (e) 1^C, 3^H sites O of TA coordinated with Cu(II) (H denotes hydroxyl oxygen and C denotes carboxyl oxygen)

density (SMD) continuum solvation model to obtain the precise thermodynamic data, and the SMD solvent model [35] can effectively calculate the Gibbs free energy change of solvation of particles.

Convergence parameters of the default threshold were retained (maximum force within 4.5×10^{-4} Hartrees/Bohr and root mean square (RMS) force within 3.0×10^{-4} Hartrees/Radian) to obtain optimized structure. The optimal structure was identified given that all calculations for structural optimization were successfully converged within the convergence threshold of no imaginary frequency, during the process of vibration analysis. On the basis of the optimized structure, bond length, bond angle, Mayer bond order, thermodynamic Gibbs free energy, and frontier molecular orbitals were analyzed in detail. Natural population analysis (NPA) was also performed to obtain the charge of Cu in the investigated systems. The electron localization function (ELF), electrostatic potential (ESP), and contribution of copper atom in frontier molecular orbitals were obtained from electronic wavefunction analysis software Multiwfn [36]. Interaction energy was calculated using Eq. (1), where m is the coordination number of TA^{2-} and Cu(II). Band gaps from the highest occupied molecular orbital (HOMO) and lowest unoccupied molecular orbital (LUMO) were calculated using Eq. (2). Based on the calculated data, hydration numbers for Cu−TA complex were predicted.

$$\Delta G=G([\mathrm{Cu(TA)}_m]^{2-2m})-(mG(\mathrm{TA}^{2-})+G(\mathrm{Cu}^{2+})) \quad (1)$$

$$(\mathrm{HOMO-LUMO})_{\mathrm{gap}}=E_{\mathrm{LUMO}}-E_{\mathrm{HOMO}} \quad (2)$$

3 Results and discussion

3.1 Experimental results

3.1.1 UV−Vis results

Selecting the appropriate absorption position to identify the measured component is very important [27,29]. Figures 2(a, c) both show that

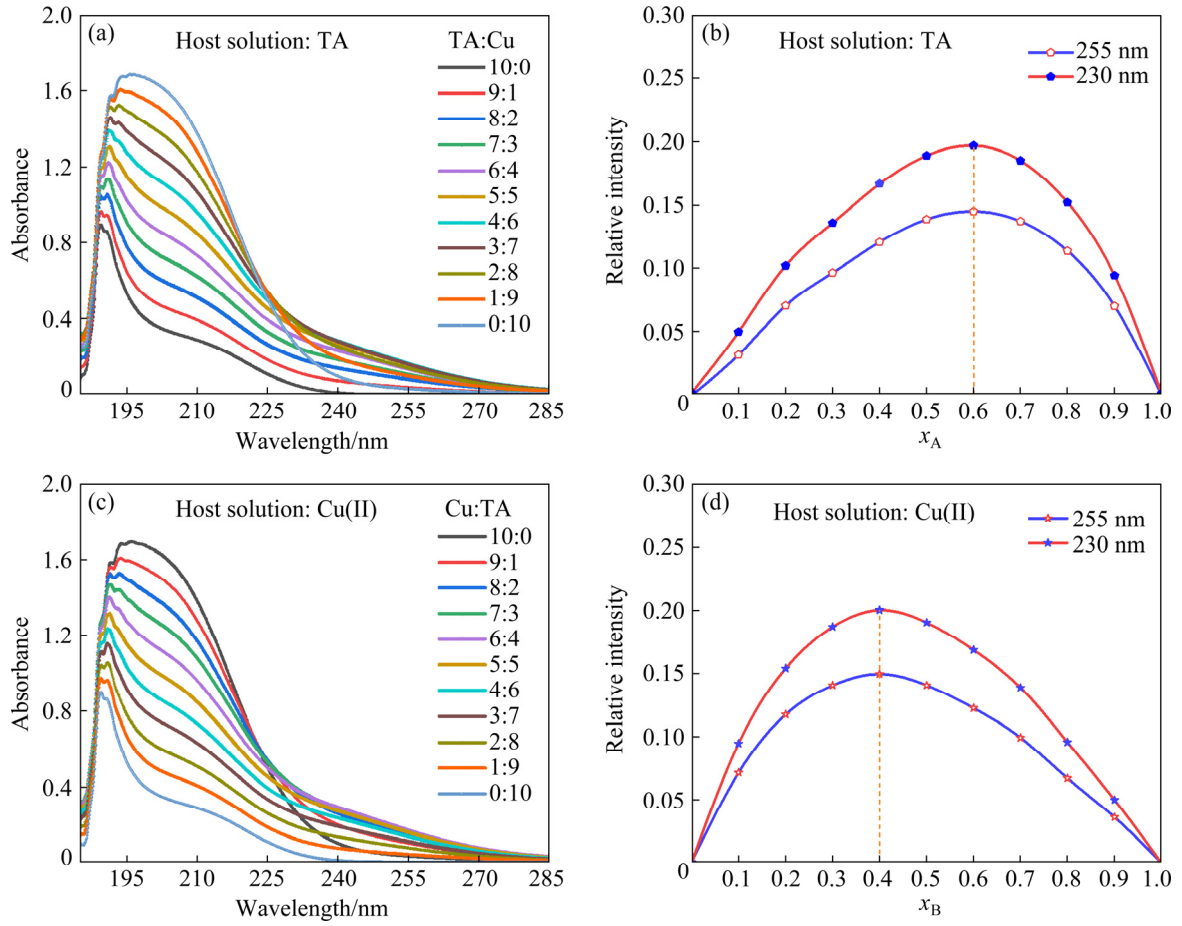

Fig. 2 UV−Vis absorbance spectra spanning wavelength from 185 to 285 nm for different dosing strategies (a, c) and corresponding Job plots at 230 and 255 nm (b, d) (x_A and x_B are the mole fractions of Cu(II) and TA according to dosing strategies 1 and 2, respectively; all stock solutions are prepared at 1 mmol/L concentration)

the increasing dosage of Cu(II) strengthens and extends the absorbance peaks. The peak strength is directly affected by the concentration of Cu(II) in a limited wavelength range (200−220 nm). However, the wavelength at 220 nm represents significant changes in solution components. Hence, selecting the changed part is important in the analysis and discussion of Cu−TA complex.

Herein, the concentration of Cu−TA complex, as determined by the integration of the intensity of a specific wavelength, was plotted against mole fraction x_A (host solution is the TA solution) and x_B (host solution is the Cu(II) solution). Moreover, the guest and host solutions were changed to understand the stoichiometry of the product comprehensively. Thus, the absorbance with wavelengths at 230 and 255 nm was selected as the monitoring physical property in Job plots shown in Figs. 2(b, d). Job plots show that x_A=0.67 when the binding stoichiometry is 1:2 and x_A=0.5 when the binding stoichiometry is 1:1 [28]. Therefore, the maximum position at x_A=0.6 identified by the inspection analysis provides the following stoichiometry of Cu(II):TA between 1:1 and 1:2. Moreover, the maximum position at x_B=0.4 further confirms the above conjecture again. In summary, these results support the formation of [Cu(TA)] and $[Cu(TA)_2]^{2-}$ complexes.

Accordingly, improved experimental evidence was collected using the liquid chromatography/mass spectrometer (LC−MS) characterization technique based on the above cognition and understanding.

3.1.2 LC−MS results

Different stoichiometric ratios were used to consider the possibility of stepwise coordination between TA and Cu(II), with molar ratios of 1:1 and 1:3. As shown in Figs. 3(a, b), the coordination results all include the single, two, and three coordination configurations of Cu−TA and water molecules also partially participate in coordination process. Common products with the relative molecular mass-to-charge ratios of 323, 362, and 423 are ascribed to $[Cu_2(TA)_3(H_2O)_2(OH)_2]^{2+}$, $[Cu(TA)_2]^+$, and $[Cu_2(TA)_2]^+$, respectively. The peak intensity of single coordination (423) decreases while peak intensity of high coordination (323, 362) increases with the increase of TA content, possibly because the single coordination content decreases and the high coordination content increases than before when TA is the host solution. Meanwhile, the weakened coordination effect of water molecules may be due to the sufficient content of TA to compete for the coordination between Cu(II) and H_2O that forms the coordination result of Cu(II) and TA instead of H_2O. The inset in Fig. 3 shows that the predicated spectra of $[Cu_2(TA)_2]^+$ and $[Cu(TA)_2]^+$ are in good agreement with the experimental results, thereby further suggesting the existence of single and high coordinated complexes. These findings are consistent with the results obtained from the Job plot analysis with UV−Vis tests.

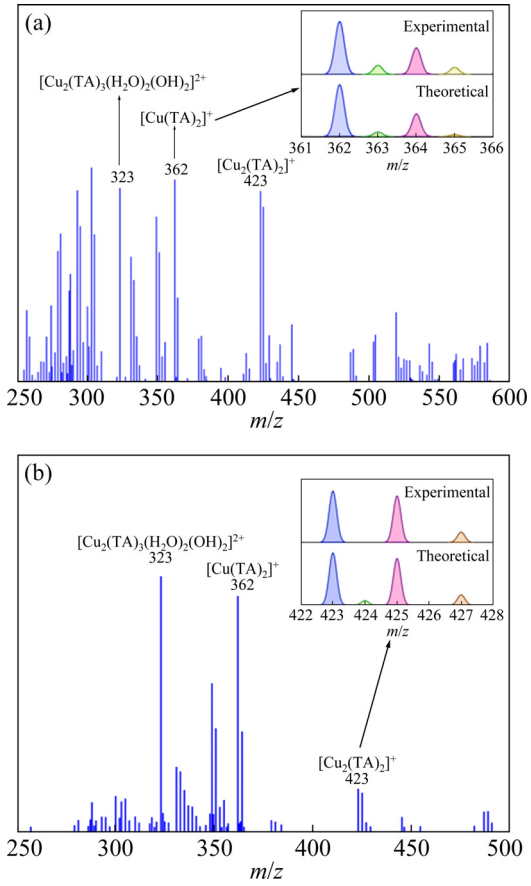

Fig. 3 LC−MS results of mixture: (a) Cu:TA molar ratio of 1:1; (b) Cu:TA molar ratio of 1:3 (The inset is the comparative results of the theoretical spectra and the experimental spectra; solution concentration of Cu(II) is 0.25 mmol/L)

3.2 Theoretical calculations

3.2.1 Single-chelating-coordination complexes

Comprehensive and systematic theoretical calculations are necessary to deeply reveal the coordination configurations and electronic properties of cupric tartrate. Figure 4 shows the electrostatic potential and its distribution of tartaric

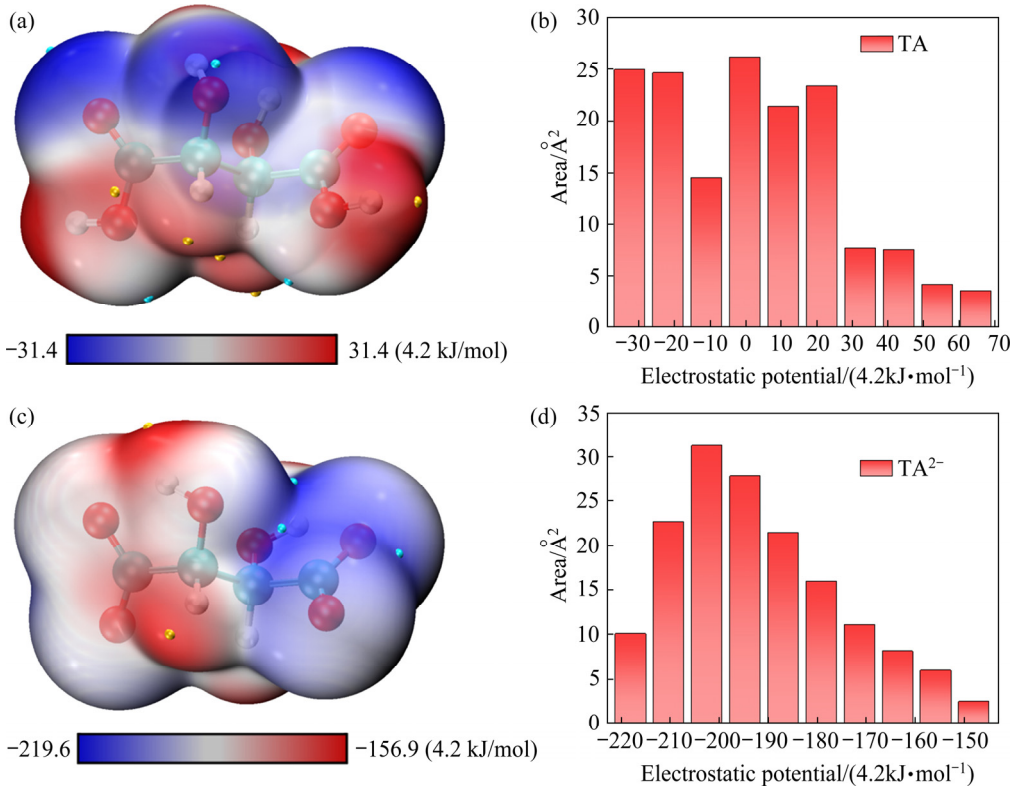

Fig. 4 Electrostatic potential diagrams (a, c) and quantitative distributions of electrostatic potential (b, d) of TA (a, b) and TA^{2-} (c, d) (Isovalue: 0.001; color scale data range: from −0.03 to 0.03; the cyan, red, and white spheres represent C O, and H atoms, respectively; the yellow and cyan sphere correspond to the maximum and minimum of electrostatic potential on the electron density isosurface, respectively)

acid before and after dehydrogenation. Before the dehydrogenation, the maximally negative electrostatic potential is mainly concentrated in the double-bond oxygen atom of the carboxyl group and the electrostatic potential of the hydroxyl group of the carboxyl group is positive. Therefore, the double-bonded oxygen atom of the carboxyl group is a favorable position for forming a coordination bond with a metal cation, specifically the Cu(II). The distribution of the electrostatic potential of TA is relatively homogeneous, and the positive potential region is slightly larger than the negative potential region. The electrostatic potential of TA^{2-} is generally negative and the favorable coordination position after dehydrogenation still needs to be systematically explored according to the actual situation.

As shown in Fig. 5(a), different coordination sites and the ionization of hydrogen ions in the carboxyl group of TA are considered into the coordination between TA and Cu(II). The length of Cu—O bond and the angle of O—Cu—O increase and the structure is more compact, reasonable, and with stronger symmetry after the dehydrogenation of carboxyl group. This phenomenon is due to, in the presence of hydrogen ions in the carboxyl group, the stronger electrostatic repulsion between the oxygen atom and copper coordination that slightly increases the Cu—O bond length and slightly decreases the O—Cu—O bond angle. However, the ionization of hydrogen ions improves the coordination ability of oxygen atoms with Cu(II) and stabilizes the structure of complexes. Furthermore, the electronegativity of coordination atoms increases and the coordination interaction with Cu(II) also intensifies in the deproton system. Structural differences between the two oxygen atoms of the carboxyl group are narrowed due to the removal of hydrogen ions. Therefore, the structure and energy of two-coordination D and E type [Cu(TA)] complexes are basically the same.

In thermodynamics, the reaction with the minimum Gibbs free energy (ΔG) can be the maximally stable and efficient one. Obviously, as shown in Fig. 6(a), the absolute value of ΔG increases significantly, and coordination structures

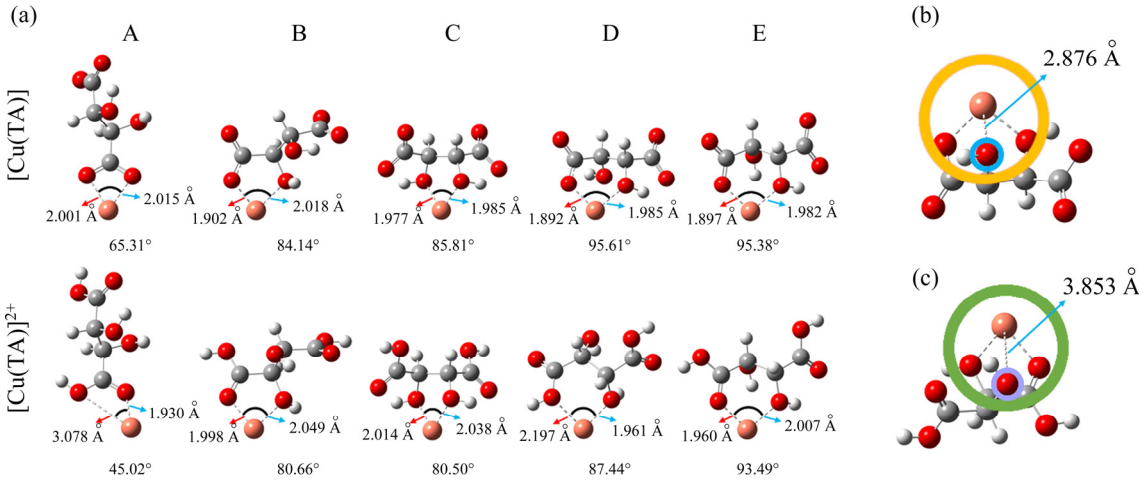

Fig. 5 Optimized structure of tartaric acid coordinated with Cu(II) before and after carboxyl dehydrogenation (a), D type [Cu(TA)] (b), and B type $[Cu(TA)]^{2+}$ (c)

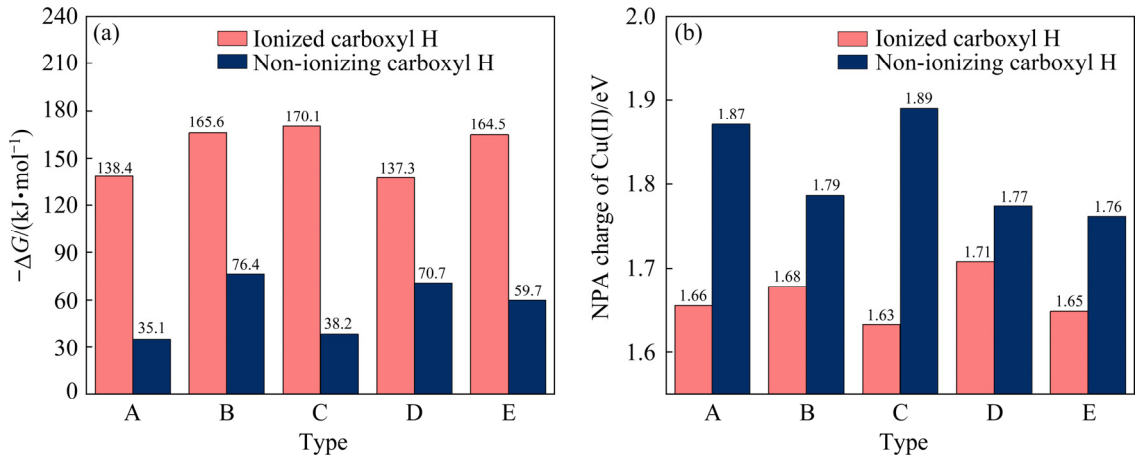

Fig. 6 Coordination of tartaric acid with Cu(II) before and after dehydrogenation: (a) Changes of Gibbs free energy; (b) Changes in NPA charge of Cu(II)

of B, D, and E types are more stable than A and C after dehydrogenation of the carboxyl group. More detailed information on Cu−TA complex can be obtained from the specialized TA^{2-}. Among them, the ΔG of D type is the smallest and it is most likely to form when TA^{2-} and Cu(II) are in the single coordination configuration. As shown in Fig. 5(b), the D type is more compact and suitable for Cu—O bond and the O—Cu—O angle after optimization, and the hydroxyl oxygen of the second carbon exerts a certain bonding effect with Cu(II) (Cu—O bond length is 2.876 Å). By contrast, the B type $[Cu(TA)]^{2+}$ demonstrates maximum stability while the Cu—O bond length is 3.853 Å when the carboxyl group is not dehydrogenated in Fig. 5(c). The NPA charge of Cu(II) in the same type of coordination structure significantly reduces after dehydrogenation in Fig. 6(b). It tends to be more stable for the coordination system of D and the NPA charges of Cu(II) are 1.89 and 1.63 eV before and after dehydrogenation, respectively.

Within the range of 0 to 1, a large ELF value means that electrons are significantly localized, indicating that there is a covalent bond, a lone pair or inner shells of the atom involved [36,37]. Cu(II) is localized in the middle of the two coordinated oxygen atoms in ELF section maps of [Cu(TA)] in Fig. 7. The ELF value in the middle position of Cu(II) is small when Cu(II) chelates with two oxygen atoms to form a coordination bond. The ELF value approaches to 0 as it continues to away from the Cu(II), where the electrons are highly delocalized. By contrast, the oxygen atom shows a large ELF value (about 0.85) with highly localized electrons due to the lone pair electrons around oxygen atoms and the covalent bond between

oxygen atoms and carbon atoms. This finding directly reveals the nature of Cu—O coordination bond, and the results are consistent with the physical meaning of ELF.

The electron cloud distributions in frontier molecular orbitals require further investigation to determine the coordination essence of B and D type [Cu(TA)]. As presented in Fig. 8(a), the electron cloud for TA^{2-} is evenly distributed, which mainly due to the high symmetry of tartaric acid molecules and its HOMO−$LUMO_{gap}$ of 11.897 eV is the largest among the three. The HOMO orbital energy for B and D type [Cu(TA)] is a lower negative value while the LUMO orbital energy is a higher positive value. That is to say, corresponding molecules and complexes are stable and predicted coordination structures are reasonable. Nucleophilic reaction can easily occur for TA^{2-} while the empty orbital around Cu(II) indicates its susceptibility to the electrophilic reaction. Meanwhile, the copper

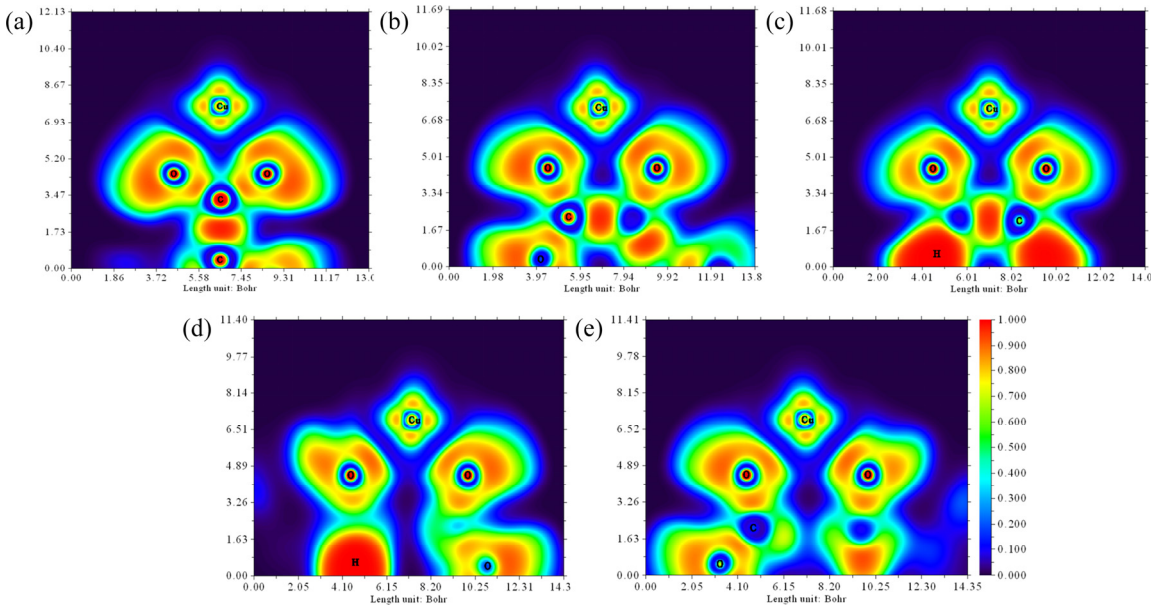

Fig. 7 Section maps of ELF: (a) A type [Cu(TA)]; (b) B type [Cu(TA)]; (c) C type [Cu(TA)]; (d) D type [Cu(TA)]; (e) E type [Cu(TA)]

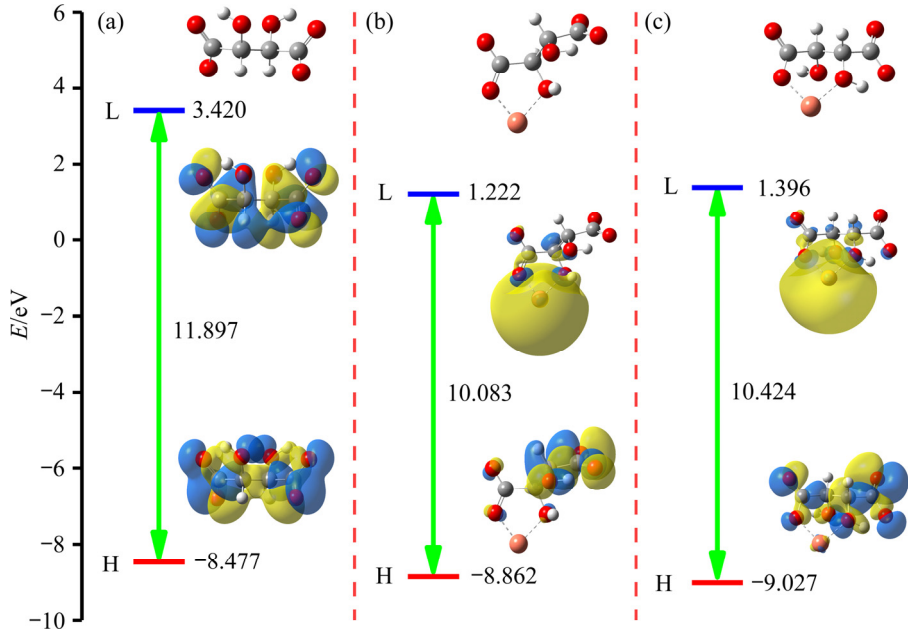

Fig. 8 Frontier molecular orbitals, energy, and energy level differences: (a) TA^{2-}; (b) B type [Cu(TA)]; (c) D type [Cu(TA)] (Yellow and blue contours are positive and negative phase orbitals, respectively, at isovalue of 0.02 a.u.)

coordination atom exerts a certain influence on the molecular structure of TA^{2-} and the orbital energy and HOMO−$LUMO_{gap}$ both reduce after coordination. The D type [Cu(TA)] with lower ΔG demonstrates a correspondingly higher energy difference than B type [Cu(TA)]. The electron cloud around the copper atom in the LUMO orbital is widely distributed and closely related to the empty orbital of Cu(II) in Figs. 8(b, c). Furthermore, the Cu(II) can easily accept electrons and undergo electrophilic reaction, thereby confirming the possibility of coordination between Cu(II) and the oxygen atom in TA^{2-}.

Cu(II) still possesses the ability to accept electrons after it accepts the electron provided by TA^{2-} to form a coordination bond, which is due to the large number of vacancies on the LUMO orbital of [Cu(TA)]. Consequently, high chelating coordination complexes are investigated.

3.2.2 High-chelating-coordination complexes

Copper complexes prefer high coordination, especially in four and even six coordination [38]. Major possible coordination configurations based on four kinds of coordination structures of the single coordination [Cu(TA)] are shown in Fig. 9. The coordination relationship is given in Eq. (3), and relevant data of thermodynamic ΔG for various possible coordination conditions are presented in Tables S1 and S2.

$$[Cu(TA)]+TA^{2-}\rightarrow[Cu(TA)_2]^{2-}+TA^{2-}\rightarrow [Cu(TA)_3]^{4-} \quad (3)$$

Based on the [Cu(TA)] coordination, the main $[Cu(TA)_2]^{2-}$ and $[Cu(TA)_3]^{4-}$ coordination configurations may be BB, BC, BD, CCC, and DDD type. The Cu(II) chelate with four oxygen atoms typically forms a plane structure and the effective expansion of plane quadrilateral is shown in Fig. 9(f), or a square-like structure for $[Cu(TA)_2]^{2-}$ coordination. $[Cu(TA)_3]^{4-}$ generally forms a spatial structure with six oxygen atoms around Cu(II) on the basis of $[Cu(TA)_2]^{2-}$ called stretched octahedron, and its spatial effective expansion is shown in Fig. 9(g). Hence, carboxylic oxygen and hydroxyl oxygen of the tartaric acid molecule are acceptable sites for Cu(II) to coordinate with. Notably, satisfactory coordination sites can also be considered as important sites for ligand degradation. Dissociation will proceed efficiently because coordination sites of Cu(II) and TA^{2-} are effectively attacked. At the same time, the selection of high-efficiency vulcanizing agents is also expected to realize the dissociation of the complex and the recovery of copper resources [39,40]. Consequently, the coordination configuration plays an important role in the degradation of heavy metal−organic complexes and the recovery of metal ions.

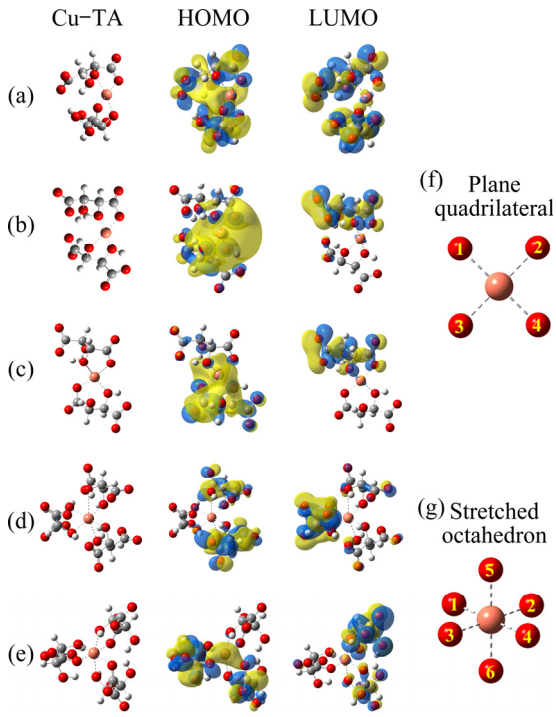

Fig. 9 Optimized structure and electron cloud distribution of frontier molecular orbitals of cupric tartrate for major two and three-coordination configurations: (a) BB type $[Cu(TA)_2]^{2-}$; (b) BC type $[Cu(TA)_2]^{2-}$; (c) BD type $[Cu(TA)_2]^{2-}$; (d) CCC type $[Cu(TA)_3]^{4-}$; (e) DDD type $[Cu(TA)_3]^{4-}$; (f) Effective expansion of plane of two-coordination complexes; (g) Effective expansion of spatial of three-coordination complexes

D type [Cu(TA)], BB type $[Cu(TA)_2]^{2-}$, and CCC type $[Cu(TA)_3]^{4-}$ are the optimal single, two, and three coordination configurations, respectively, based on ΔG from the perspective of stepwise coordination in Table 1. Although these stable coordination structures can prevent the hydrolysis of metal ions in aqueous solutions [41,42], they also intensify the difficulty in subsequent resource utilization of metal ions and organic matter and even the standard treatment of electronic industry wastewater [43,44]. As investigated using Hirshfeld's method [45], copper contributes approximately 80% to LUMO orbitals for single coordination, which can be visually reflected by the

Table 1 Gibbs free energy change of stepwise coordination, $(HOMO-LUMO)_{gap}$, and contribution of copper atoms to frontier molecular orbitals of major cupric tartrate coordination structures

Type	ΔG/(kJ·mol^{-1})	$(HOMO-LUMO)_{gap}$/eV	Contribution of copper atom to frontier molecular orbitals/%	
			HOMO	LUMO
B	−165.7	10.08	0.085	81.048
C	−137.3	10.25	0.370	78.492
D	−170.1	10.42	0.848	79.271
BB	−136.2	11.64	1.312	7.693
BC	−125.7	11.25	0.650	36.147
BD	−122.3	11.13	0.564	10.500
CCC	−90.2	11.59	0.439	1.508
DDD	−61.5	11.12	0.769	2.813

size of electron cloud around the copper atom in the frontier molecular orbitals in Fig. 7. The contributions of copper atom to LUMO orbitals decrease and reach the minimum at three-coordination configurations and those to HOMO orbitals are less variable as TA^{2-} continues to coordinate with Cu(II).

The Mayer bond order was calculated to further reveal the coordination essence of Cu—O bond and measure the logarithm of shared electrons effectively, as collected in Table 2. The Mayer bond order values of Cu—O bond demonstrate certain regularity in the two-coordination configuration; that is, the similarity of Cu—1O and Cu—4O as well as Cu—2O and Cu—3O improves the symmetry of the coordination configuration. A long Cu—O bond length corresponds to a small bond order in the case of three-coordination configuration, and especially, that of the Cu—5O and Cu—6O reaches the lower in the same type. This finding is consistent with the structure of a stretched hexahedron.

3.2.3 Effect of explicit solvents on coordination complexes

Water molecules will appear as ligands to form highly coordinated complexes with more than six coordination configurations, or replace oxygen atoms on the carboxyl to form configurations that cannot be fully coordinated [46]. Although the single coordination of [Cu(TA)] is stable, water molecules contain two lone pairs of electrons that also need to be regarded as ligands [38].

Table 2 Mayer bond order of Cu—O bond in major two and three-coordination levels of cupric tartrate

Bond	BB	BC	BD	CCC	DDD
Cu—1O	0.463	0.511	0.450	0.463	0.428
Cu—2O	0.638	0.660	0.634	0.437	0.519
Cu—3O	0.638	0.452	0.591	0.451	0.669
Cu—4O	0.463	0.467	0.454	0.476	0.438
Cu—5O	−	−	−	0.263	0.272
Cu—6O	−	−	−	0.161	0.130

The solvent interactions of water molecules were considered and multiple coordination interactions were formed on the basis of B and D type [Cu(TA)]. There are six coordination sites for Cu(II) in aqueous solutions [47,48], and thereby at most four more water molecules can be coordinated on the basis of B and D types. Furthermore, as shown in Fig. 10(a), water molecules here are successively added one by one. The corresponding ΔG and NPA charge of copper are presented in Fig. S2. Typically, a square-like structure tends to be formed and then a spatial structure between Cu(II) and the surrounding oxygen atoms. Moreover, the D type [Cu(TA)] begins to form spatial-like structure when it coordinates two water molecules mainly because TA^{2-} provides three oxygen atoms to coordinate with Cu(II), as analyzed in Fig. 5(b). The stretched octahedron and saturated coordination configuration are formed when three water molecules participate in the coordination. However, coordination of the fourth water molecule is impossible according to ΔG.

Notably, the stepwise coordination process of water molecules should be considered in detail. The reaction that occurs when Cu(II) in Cu−TA complex is successively coordinated with H_2O can be expressed as Eqs. (4)−(7):

$$[Cu(TA)] + H_2O \rightarrow [Cu(TA)(H_2O)] \quad (4)$$

$$[Cu(TA)(H_2O)] + H_2O \rightarrow [Cu(TA)(H_2O)_2] \quad (5)$$

$$[Cu(TA)(H_2O)_2] + H_2O \rightarrow [Cu(TA)(H_2O)_3] \quad (6)$$

$$[Cu(TA)(H_2O)_3] + H_2O \rightarrow [Cu(TA)(H_2O)_4] \quad (7)$$

Figure 10(b) shows that coordination of the first H_2O on [Cu(TA)] is easy to occur and the absolute value of ΔG reaches the maximum in the above four equations. The absolute value of ΔG

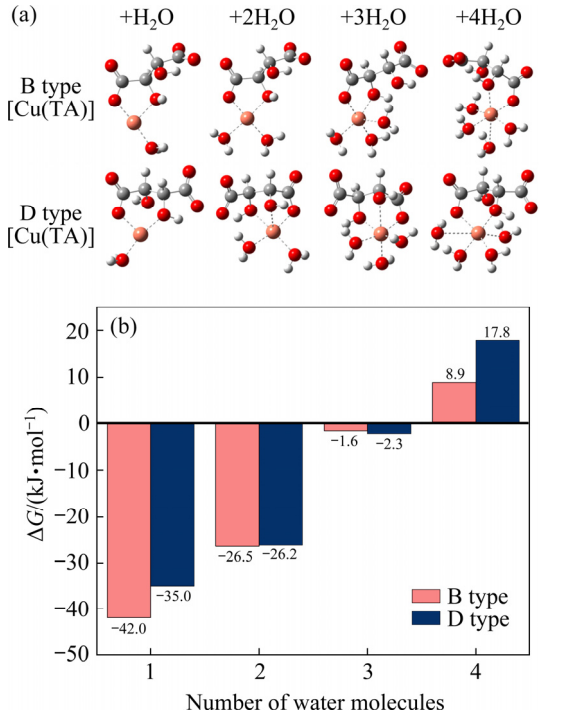

Fig. 10 Optimized results of Cu(II) coordinated with H_2O on basis of B and D type [Cu(TA)] complexes (a), and Gibbs free energy change of stepwise coordination of B and D type [Cu(TA)] complexes with H_2O (b)

decreases as the second H_2O is coordinated. ΔG approaches to zero as the third H_2O is considered, indicating that Eq. (6) is difficult to occur. The chelation of B and D type [Cu(TA)] with the fourth H_2O fails to occur because ΔG is already positive. Furthermore, three oxygen atoms in TA^{2-} coordinated with Cu(II) exert a serious steric hindrance effect on water molecules. Structurally, the bond length of Cu—O between Cu(II) and H_2O significantly increases. Therefore, three H_2O have basically reached the limit when water molecules are coordinated on the basis of [Cu(TA)].

Coordinating a maximum of two water molecules is possible because four oxygen atoms are coordinated with Cu(II) for the two-coordination configuration. The positive change in ΔG is caused by the coordination reaction between BB type $[Cu(TA)_2]^{2-}$ and H_2O, as shown in Fig. 11, implicating that the binding of the water molecule with the former is unfavorable in thermodynamics. Nevertheless, as shown in Fig. S3, intramolecular hydrogen bonds (O—H···O) that occur between the added H_2O and TA^{2-} enable the easier coordination of BC and BD types with the second H_2O than the first one.

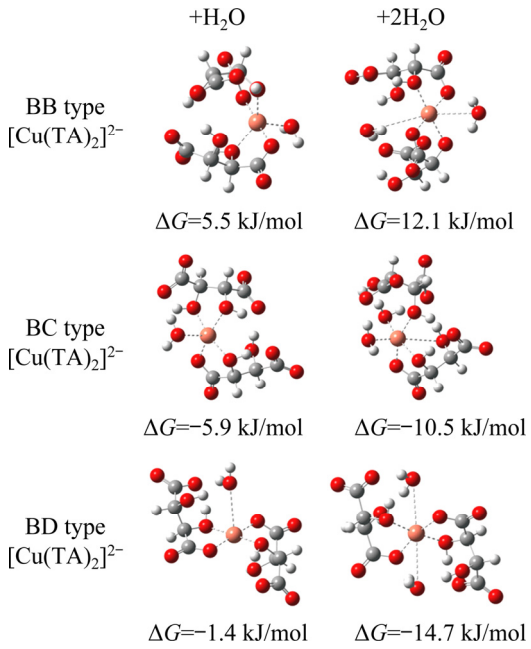

Fig. 11 Optimized results of Cu(II) coordinated with H_2O on basis of BB, BC, and BD type $[Cu(TA)_2]^{2-}$

4 Conclusions

(1) Job plots drawn at 230 and 255 nm based on UV–Vis results consistently show the possible existence of [Cu(TA)] and $[Cu(TA)_2]^{2-}$ complexes.

(2) LC–MS results provide strong evidence that $[Cu_2(TA)_2]^{+}$, $[Cu(TA)_2]^{+}$, and $[Cu_2(TA)_3(H_2O)_2(OH)_2]^{2+}$ are stably present in the aqueous solution and water molecules are involved in the coordination process as ligands.

(3) DFT calculations show that [Cu(TA)] (1^{H}, 3^{H} sites O of TA coordinated with Cu(II)), $[Cu(TA)_2]^{2-}$ (two 1^{C}, 2^{H} sites O of TA coordinated with Cu(II)), and $[Cu(TA)_3]^{4-}$ (three 2^{H}, 3^{H} sites O of TA coordinated with Cu(II)) should be the dominant coordination configurations, with Gibbs free energies of −170.1, −136.2, and −90.2 kJ/mol, respectively.

(4) A maximum of three water molecules can be coordinated on the basis of the single coordination [Cu(TA)], and two water molecules can be coordinated on the basis of two-coordination $[Cu(TA)_2]^{2-}$.

(5) This work could provide new insights into the optimal design of active molecules in electroplating solution and the effective treatment of copper containing electronic industrial wastewater.

Supplementary information

Supplementary information in this paper can be found at: http://www.ysxbcn.com/download/20-p3753-2021-1102-Supplementary_information.pdf.

Acknowledgments

This work was financially supported by the National Key Research and Development Program of China (No. 2019YFC0408303), the Natural Science Foundation of Hunan Province, China (No. 2021JJ20069), the Changsha Science and Technology Project, China (Nos. kq2106016, kq2009005), Higher Education Discipline Innovation Project (111 Project), China (No. B14034), and the Fundamental Research Funds for the Central Universities of Central South University, China (No. 2021zzts0887). This work was carried out in part using hardware and/or software provided by a Tianhe II supercomputer at the National Supercomputing Center in Guangzhou, Computing Platform of Mineral Processing Computational Chemistry of School of Mineral Processing and Bioengineering of Central South University (China), and the High Performance Computing Centers of Central South University (China).

References

[1] ZHANG Bing-gang, ZHAO Jian, LI Xiao-peng, FENG Ji-cai. Electron beam welding of 304 stainless steel to QCr0.8 copper alloy with copper filler wire [J]. Transactions of Nonferrous Metals Society of China, 2014, 24(12): 4059−4066.

[2] LI Zheng, CHANG Shu-quan, KHUJE S, REN Shen-qiang. Recent advancement of emerging nano copper-based printable flexible hybrid electronics [J]. Acs Nano, 2021, 15(4): 6211−6232.

[3] KRAMER R. Fluorescent chemosensors for Cu^{2+} ions: Fast, selective, and highly sensitive [J]. Angewandte Chemie (International ed in English), 1998, 37(6): 772−773.

[4] CHAI Li-yuan, PENG Cong, MIN Xiao-bo, TANG Chong-jian, SONG Yu-xia, ZHANG Yang, ZHANG Jing, ALI M. Two-sectional struvite formation process for enhanced treatment of copper-ammonia complex wastewater [J]. Transactions of Nonferrous Metals Society of China, 2017, 27(2): 457−466.

[5] YE Qian, XU Hao, WANG Qing-guo, HUO Xiao-wei, WANG Yun-qi, HUANG Xue, ZHOU Guan-yu, LU Jin-feng, ZHANG Jing. New insights into the mechanisms of tartaric acid enhancing homogeneous and heterogeneous copper-catalyzed Fenton-like systems [J]. Journal of Hazardous Materials, 2021, 407: 13.

[6] YOUNES M, AQUILINA G, CASTLE L, ENGEL K H, FOWLER P, FERNANDEZ M J F, FURST P, GURTLER R, GUNDERT-REMY U, HUSOY T, MENNES W, SHAH R, WAALKENS-BERENDSEN I, WOELFLE D, BOON P, TOBBACK P, WRIGHT M C, AGUILERA J, RINCON A M, TARD A, MOLDEUS P. Re-evaluation of L(+)-tartaric acid (E 334), sodium tartrates (E 335), potassium tartrates (E 336), potassium sodium tartrate (E 337) and calcium tartrate (E 354) as food additives [J]. EFSA Journal, 2020, 18(3): e06030.

[7] JUNSONGDUANG A, SIRITHIP K, INTA A, NACHAI R, ONPUTTHA B, TANMING W, BALSLEV H. Diversity and traditional knowledge of textile dyeing plants in northeastern Thailand [J]. Economic Botany, 2017, 71(3): 241−255.

[8] WANG Bei-bei, YU Wei-wei, GUO Jia-wei, JIANG Xing-wu, LU Wei-qiang, LIU Ming-yao, PANG Xiu-feng. The antiparasitic drug, potassium antimony tartrate, inhibits tumor angiogenesis and tumor growth in nonsmall-cell lung cancer [J]. Journal of Pharmacology and Experimental Therapeutics, 2015, 352(1): 129−138.

[9] JASTRZAB R, KACZMAREK M, NOWAK M, TROJANOWSKA A, ZABISZAK M. Complexes of polyamines and their derivatives as living system active compounds [J]. Coordination Chemistry Reviews, 2017, 351: 32−44.

[10] ZELENINA T E, ZELENIN O Y. Complexation of citric and tartaric acids with Na and K ions in aqueous solution [J]. Russian Journal of Coordination Chemistry, 2005, 31(4): 235−242.

[11] HU Jing, LU Feng-ting, DING Li-ping, ZHANG Shu-juan, FANG Yu. A novel pyrene-based film: Preparation, optical properties and sensitive detection of organic copper(II) salts [J]. Journal of Photochemistry and Photobiology a−Chemistry, 2007, 188(2/3): 351−357.

[12] PARRY R W, DUBOIS F W. Citrate complexes of copper in acid solutions [J]. Journal of the American Chemical Society, 1952, 74(15): 3749−3753.

[13] LIU Xin-xiu, WANG Ying-hua, SUN Xian-bo, LIU Yong-di. Study on the treatment of tartaric acid-copper complex wastewater by UV/O_3 [J]. Journal of East China University of Science and Technology (Natural Science Edition), 2014, 40(6): 718−722, 745. (in Chinese)

[14] WANG Dan-dan, YANG Bo-wen, YE Yu-xuan, ZHANG Wei-ming, WEI Zhong-bo. Nickel speciation of spent electroless nickel plating effluent along the typical sequential treatment scheme [J]. Science of the Total Environment, 2019, 654: 35−42.

[15] FU Feng-lian, XIE Li-ping, TANG Bing, WANG Qi, JIANG Shu-xian. Application of a novel strategy—Advanced Fenton-chemical precipitation to the treatment of strong stability chelated heavy metal containing wastewater [J]. Chemical Engineering Journal, 2012, 189/190: 283−287.

[16] GAO Jing, QIU Yun-ren, LI Mao-lin, LE Hui-shang. Removal of Co(II) from aqueous solution by complexation−ultrafiltration and shear stability of PAA−Co complex [J]. Transactions of Nonferrous Metals Society of China, 2019, 29(6): 1346−1352.

[17] SONG Lai-zhou, ZHAO Rui-fang, YUN Dan-dan, LU Ping-ping, HE Jun, WANG Xiu-li. Influence of Co(II), Ni(II), tartrate, and ethylene diaminetetra acetic acid on Cu(II)

adsorption onto a polyvinylidene fluoride-based chelating membrane [J]. Toxicological & Environmental Chemistry, 2014, 96(3): 362−378.

[18] WU Feng-chi, TSENG Ru-ling, JUANG Ruey-shin. Kinetic modeling of liquid-phase adsorption of reactive dyes and metal ions on chitosan [J]. Water Research, 2001, 35(3): 613−618.

[19] DU Jun-qun, ZHANG Bao-gang, LI Jia-xin, LAI Bo. Decontamination of heavy metal complexes by advanced oxidation processes: A review [J]. Chinese Chemical Letters, 2020, 31(10): 2575−2582.

[20] NGUYEN M K, TRAN V S, PHAM T T, PHAM H G, HOANG B L, NGUYEN T H, NGUYEN T H, TRAN T H, NGO H H. Fenton/ozone-based oxidation and coagulation processes for removing metals (Cu,Ni)-EDTA from plating wastewater [J]. Journal of Water Process Engineering, 2021, 39: 101836.

[21] WONG K K, LEE C K, LOW K S, HARON M J. Removal of Cu and Pb by tartaric acid modified rice husk from aqueous solutions [J]. Chemosphere, 2003, 50: 23−28.

[22] LEONELLO R, SAVIO M, TOALDO P B, BONOMI R. New procedure to readily investigate lactase enzymatic activity using Fehling's reagent [J]. Journal of Chemical Education, 2018, 95(7): 1238−1242.

[23] LI Tian, ZHOU Dian-wu, YAN You-rui-ling, PENG Ping, LIU Jin-shui. First-principles and experimental investigations on ductility/brittleness of intermetallic compounds and joint properties in steel/aluminum laser welding [J]. Transactions of Nonferrous Metals Society of China, 2021, 31(10): 2962−2977.

[24] AGHAEI S M, AASI A, FARHANGDOUST S, PANCHAPAKESAN B. Graphene-like BC6N nanosheets are potential candidates for detection of volatile organic compounds (VOCs) in human breath: A DFT study [J]. Applied Surface Science, 2021, 536: 13.

[25] HU Bin, YANG Tian-zu, LIU Wei-feng, ZHANG Du-chao, CHEN Lin. Removal of arsenic from acid wastewater via sulfide precipitation and its hydrothermal mineralization stabilization [J]. Transactions of Nonferrous Metals Society of China, 2019, 29(11): 2411−2421.

[26] XU Shao-dong, LI Dong, GUO Xue-yi, YAN Wen, GAO Jie. Selenium(VI) removal from caustic solution by synthetic Ca−Al−Cl layered double hydroxides [J]. Transactions of Nonferrous Metals Society of China, 2019, 29(8): 1763−1775.

[27] WANG Tie-cheng, CAO Yang, QU Guang-zhou, SUN Qiu-hong, XIA Tian-jiao, GUO Xue-tao, JIA Han-zhong, ZHU Ling-yan. Novel Cu(II)–EDTA decomplexation by discharge plasma oxidation and coupled cu removal by alkaline precipitation: Underneath mechanisms [J]. Environmental Science & Technology, 2018, 52(14): 7884−7891.

[28] RENNY J S, TOMASEVICH L L, TALLMADGE E H, COLLUM D B. Method of continuous variations: Applications of Job plots to the study of molecular associations in organometallic chemistry [J]. Angewandte Chemie-International Edition, 2013, 52(46): 11998−12013.

[29] HE Jian-yong, HAN Hai-sheng, ZHANG Chen-yang, HU Yue-hua, YUAN Dan-dan, TIAN Meng-jie, CHEN Dai-xiong, SUN Wei. New insights into the configurations of lead(II)-benzohydroxamic acid coordination compounds in aqueous solution: A combined experimental and computational study [J]. Minerals, 2018, 8(9): 368.

[30] CHEN Tao, ZHANG Qin, LI Zhi, YIN Xian-hua, HU Fang-rong. Experimental and theoretical investigations of tartaric acid isomers by terahertz spectroscopy and density functional theory [J]. Spectrochimica Acta Part A: Molecular and Biomolecular Spectroscopy, 2018, 205: 312−319.

[31] YAN Hui-Juan, WANG Dong, HAN Mei-Juan, WAN Li-Jun, BAI Chun-Li. Adsorption and coordination of tartaric acid enantiomers on Cu(111) in aqueous solution [J]. Langmuir, 2004, 20(18): 7360−7364.

[32] FRISCH M J, TRUCKS G W, SCHLEGEL H B, SCUSERIA G E, ROBB M A, CHEESEMAN J R, SCALMANI G, BARONE V, PETERSSON G A, NAKATSUJI H, LI X, CARICATO M, MARENICH A V, BLOINO J, JANESKO B G, GOMPERTS R, MENNUCCI B, HRATCHIAN H P, ORTIZ J V, IZMAYLOV A F, SONNENBERG J L, WILLIAMS-YOUNG D, DING F, LIPPARINI F, EGIDI F, GOINGS J, PENG B, PETRONE A, HENDERSON T, RANASINGHE D, ZAKRZEWSKI V G, GAO J, REGA N, ZHENG G, LIANG W, HADA M, EHARA M, TOYOTA K, FUKUDA R, HASEGAWA J, ISHIDA M, NAKAJIMA T, HONDA Y, KITAO O, NAKAI H, VREVEN T, THROSSELL K, MONTGOMERY J A, JR, PERALTA J E, OGLIARO F, BEARPARK M J, HEYD J J, BROTHERS E N, KUDIN K N, STAROVEROV V N, KEITH T A, KOBAYASHI R, NORMAND J, RAGHAVACHARI K, RENDELL A P, BURANT J C, IYENGAR S S, TOMASI J, COSSI M, MILLAM J M, KLENE M, ADAMO C, CAMMI R, OCHTERSKI J W, MARTIN R L, MOROKUMA K, FARKAS O, FORESMAN J B, J. Fox D. Gaussian 16, Revision A.03 [Z]. Gaussian, Inc., Wallingford CT, 2016.

[33] CHAI Jeng-Da, HEAD-GORDON M. Long-range corrected hybrid density functionals with damped atom-atom dispersion corrections [J]. Physical Chemistry Chemical Physics, 2008, 10(44): 6615−6620.

[34] GRIMME S. Semiempirical GGA-type density functional constructed with a long-range dispersion correction [J]. Journal of Computational Chemistry, 2006, 27(15): 1787−1799.

[35] MARENICH A V, CRAMER C J, TRUHLAR D G. Universal solvation model based on solute electron density and on a continuum model of the solvent defined by the bulk dielectric constant and atomic surface tensions [J]. Journal of Physical Chemistry B, 2009, 113(18): 6378−6396.

[36] LU Tian, CHEN Fei-wu. Multiwfn: A multifunctional wavefunction analyzer [J]. Journal of Computational Chemistry, 2012, 33(5): 580−592.

[37] BECKE A D, EDGECOMBE K E. A simple measure of electron localization in atomic and molecular-systems [J]. Journal of Chemical Physics, 1990, 92(9): 5397−5403.

[38] PAVELKA M, BURDA J V. Theoretical description of copper Cu(I)/Cu(II) complexes in mixed ammine-aqua environment. DFT and *ab initio* quantum chemical study [J]. Chemical Physics, 2005, 312(1/2/3): 193−204.

[39] HE Jian-yong, ZHANG Chen-yang, SONG Shao-le, SUN Wei, HU Yue-hua, LEI Shu-ya, YANG Yue. Computational

and experimental investigation of dimethyldithiocarbamate for effective recovery of cobalt and nickel from the leach liquor of high manganese slag [J]. Separation and Purification Technology, 2019, 223: 55−62.

[40] CHEN Hui, ZHAO Yue, YANG Qiu-yu, YAN Qun. Preparation of poly-ammonium/sodium dithiocarbamate for the efficient removal of chelated heavy metal ions from aqueous environments [J]. Journal of Environmental Chemical Engineering, 2018, 6(2): 2344−2354.

[41] AABOUBI O, HOUSNI A. Thermoelectrochemical study of silver electrodeposition from nitric and tartaric solutions [J]. Journal of Electroanalytical Chemistry, 2012, 677/678/679/680: 63−68.

[42] BERES M, SYZDEK J, YU K M, MAO S S. Growth behavior of co-electrodeposited CZTS precursor thin films from acidic baths containing tartaric acid [J]. Materials Chemistry and Physics, 2018, 204: 83−94.

[43] AJIBOYE T O, OYEWO O A, ONWUDIWE D C. Simultaneous removal of organics and heavy metals from industrial wastewater: A review [J]. Chemosphere, 2021, 262: 128379.

[44] LIAO Zhen-liang, ZHAO Zhi-chao, ZHU Jing-cheng, CHEN Hao, MENG Dai-zong. Complexing characteristics between Cu(II) ions and dissolved organic matter in combined sewer overflows: Implications for the removal of heavy metals by enhanced coagulation [J]. Chemosphere, 2021, 265: 129023.

[45] BULTINCK P, C Van A, AYERS P W, CARBO-DORCA R. Critical analysis and extension of the Hirshfeld atoms in molecules [J]. Journal of Chemical Physics, 2007, 126(14): 144111.

[46] WANDER M C F, CLARK A E. Hydration properties of aqueous Pb(II) ion [J]. Inorganic Chemistry, 2008, 47(18): 8233−8241.

[47] HAY P J, WADT W R. *Ab initio* effective core potentials for molecular calculations: Potentials for the transition metal atoms Sc to Hg [J]. Journal of Chemical Physics, 1985, 82: 270.

[48] LI Xiao-hui, XUE Han, ZHANG Lan-cui, ZHU Zai-ming. Hydrothermal synthesis and crystal structure of mononuclear and binuclear copper tartrate complexes [J]. Chemical Reagents, 2010, 32(6): 537−540, 544. (in Chinese)

电子工业废水中酒石酸铜的配位构型

韩明君[1]，何建勇[1]，孙 伟[1]，李 赛[1]，余 恒[1]，岳 彤[1]，魏 鑫[2]，张晨阳[1,3,4]

1. 中南大学 矿物加工与生物工程学院 战略含钙矿产资源清洁高效利用湖南省重点实验室，长沙 410083；
2. 苏州东方环境工程有限公司，苏州 215110；
3. 湖南省有色金属研究院 复杂铜铅锌伴生金属资源综合利用湖南省重点实验室，长沙 410100；
4. 昆明理工大学 省部共建复杂有色金属资源清洁利用国家重点实验室，昆明 650093

摘 要：采用紫外可见光谱(UV−Vis)和液相色谱/质谱(LC−MS)分析酒石酸铜(Cu−TA)配合物的配位结构，并通过密度泛函理论(DFT)计算系统地揭示酒石酸铜在水溶液中的有效配位构型和电子特性。UV−Vis 在 230 和 255 nm 处的 Job 图一致显示可能存在[Cu(TA)]和$[Cu(TA)_2]^{2-}$。LC−MS 结果证实单配位和高配位配合物$[Cu_2(TA)_2]^{+}$、$[Cu(TA)_2]^{+}$和$[Cu_2(TA)_3(H_2O)_2(OH)_2]^{2+}$的存在。DFT 计算结果表明，酒石酸(TA)的羧基氧和羟基氧是 Cu(II)的优选配位位点。[Cu(TA)] (酒石酸分子 1 号碳的羟基氧和 3 号碳的羟基氧与 Cu(II)配位)、$[Cu(TA)_2]^{2-}$ (2 个酒石酸分子 1 号碳的羧基氧和 2 号碳的羟基氧与 Cu(II)配位)以及$[Cu(TA)_3]^{4-}$ (3 个酒石酸分子 2 号碳的羟基氧和 3 号碳的羟基氧与 Cu(II)配位)是酒石酸铜的主要配位构型。三者的吉布斯自由能分别为−170.1、−136.2 和−90.2 kJ/mol。

关键词：电子工业废水；铜；酒石酸；酒石酸铜配合物；配位构型；密度泛函理论

(Edited by Bing YANG)